Journal of Applied Physics ARTICLE scitation.org/journal/jap

Electron-beam excitation of supermodes of a photonic molecule built on twin high refractive index dielectric nanowires

Cite as: J. Appl. Phys. **125**, 223102 (2019); doi: 10.1063/1.5095722
Submitted: 12 March 2019 · Accepted: 24 May 2019 ·
Published Online: 13 June 2019

Dariia O. Yevtushenko,[a] Sergii V. Dukhopelnykov, and Alexander I. Nosich

AFFILIATIONS

Laboratory of Micro and Nano Optics, Institute of Radio-Physics and Electronics NASU, Kharkiv 61085, Ukraine

Note: This paper is part of the Special Topic on Dielectric Nanoresonators and Metamaterials.
[a]dariia.yevtushenko@gmail.com

ABSTRACT

We study the radiation that occurs if a modulated beam of electrons flows between two identical high-index dielectric nanowires, which form a photonic molecule, in the visible wavelength range. The electromagnetic field of such a two-dimensional beam has the shape of the surface wave propagating along its trajectory. This wave induces the polarization and surface currents on the nearby obstacles, and hence, radiation occurs even if the beam does not touch the obstacle. Here, a pair of dielectric nanowires behaves as optically coupled open resonators, thanks to which the diffraction radiation is enhanced near the wavelengths of the natural modes. As known, the latter are so-called supermodes built on the modes of each wire, with the account of two-fold symmetry of the pair. To solve accurately the scattering problem, we use a semianalytical technique based on the Fourier expansions in the local coordinates of each wire and the addition theorems for the cylindrical functions. This leads to the efficient code having mathematically guaranteed convergence. We compute spectral characteristics of the diffraction radiation, analyze their dependences on the electron-beam parameters, and visualize the near-field and far-field patterns. A new form of the optical theorem adapted to the modulated electron-beam excitation is derived and exploited. Possible applications of the studied effects in the design of optical beam position monitors are discussed.

I. INTRODUCTION

Photonic molecules (PMs) have been attracting the attention of researchers since the late 1990s as configurations occupying an intermediate place between photonic crystals and "photonic atoms," or standalone dielectric particles.[1–6] PMs are configured as a finite number of identical elements, usually having certain symmetry, say, a linear "chain" of them or a cyclic "necklace." They confine light and enable its efficient manipulation at the micrometer length scale due to the tight photonic binding (i.e., strong optical coupling). This is an alternative to the manipulation of light in the photonic crystals which are the media with periodic variation of refractive index and almost "free" photon propagation. The simplest PM contains two identical spherical[2] or circular-wire (Fig. 1) elements and hence it has two-fold symmetry.

This circumstance leads to the appearance of four orthogonal families of natural modes of such a twin PM.[3] Here, each mode of PM is built on a certain mode of the individual dielectric cavity, the cavities being optically coupled together in one of the four possible ways. Therefore, coupled-cavity modes are called "supermodes." Each family's supermodes possess either symmetry or antisymmetry of each field component with respect to each symmetry plane. This is usually expressed via the terms "bonding" and "antibonding" or "even" and "odd," respectively. Besides, the symmetry and antisymmetry can be understood via the placement of the virtual perfect electrically conducting (PEC) or perfect magnetically conducting (PMC) wall along the corresponding symmetry plane. Under an external illumination, say, with a plane wave, PM supermodes can be either "bright" ones, that is, display resonances in the scattering and absorption, or remain "dark." The latter happens if the incident field symmetry is different from the symmetry of the supermode natural field.

Although the bulk of research in nano-optics and photonics is performed around the excitation of dielectric nanoresonators with either plane or cylindrical waves, charged particles and beams of them can also serve as a source. As it was first found in the 1950s,

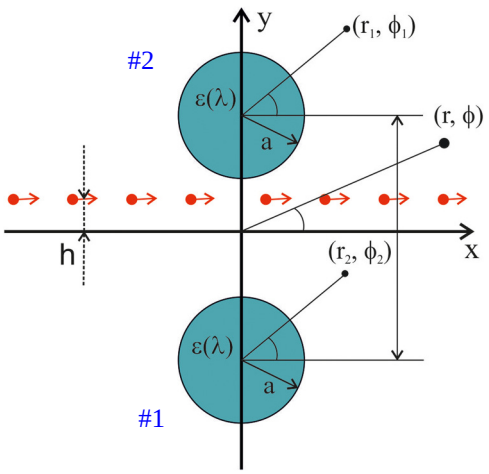

FIG. 1. Cross-sectional geometry of an electron beam moving between a pair of identical circular nanowires, which form a photonic molecule.

the electrons passing nearby a periodic structure, say, a lamellar grating, radiate the light. This effect obtained the name of its discoverers, Smith and Purcell (SPE).[7] Since then, it was actively studied both experimentally and theoretically.[7–9] Today, SPE is considered as a particular case, although perhaps the most practically important one, of a more broadly defined effect. This is the radiation of the surface and polarization currents induced on various material objects in various frequency regions by the charged particles or their beams, which do not touch or hit these material objects. In order to distinguish this type of electromagnetic-wave radiation from the others, such as, for instance, the transition radiation, it is commonly called the diffraction radiation (DR).[10–12]

Obviously, such DR is characterized by the far-field angular patterns and the radiated power that depend on the electron-beam bunching, velocity, and fine distance from the scatterers to the beam trajectory. Therefore, DR can serve as a basis for the development of beam position monitors (BPMs). Such monitors are known in the microwave range.[13–17] However, the emergence and rapid development of nanotechnology open a way to the use of nanoscale components in various optical circuits. In fact, today the design of optical-range DR-based BPMs is viewed as the most promising technique in noninvasive beam diagnostics.[18,19] Another application area is related to the novel accelerating techniques.[20]

Our goal is the exploration of the opportunity of using the PM configuration shown in Fig. 1 and its DR characteristics for obtaining the information on the beam position shift h. Nanoscale size of such sensor antennas introduces negligible distortion to the beam energy characteristics, which can be considered as fixed. This makes possible the analysis of the BPM in the same way as within the traditional electromagnetic theory, i.e., as the scattering of the given electromagnetic-wave field of the moving beam by the scatterers of given shapes and material properties. The latter parameters can be manipulated to optimize the BPM performance. Note that high refractive index dielectric nanowires can be designed resonant and, moreover, tunable if covered with the graphene.[21–24]

II. MODULATED BEAM FIELD AS A SURFACE WAVE

Consider an unbounded two-dimensional (2D) electron beam moving along the straight trajectory at the distance from h from the x axis, with a fixed velocity $v = \beta c$ (where $\beta \leq 1$). The charge density function, if modulated in time in a harmonic manner, can be presented as

$$\rho = \rho_0 \delta(y - h) \exp[i(kx/\beta - \omega t)], \tag{1}$$

where $\delta(\cdot)$ is the Dirac delta function, ω and ρ_0 are the frequency and the amplitude of the beam modulation, respectively. $k = \omega/c$ is the free-space wavenumber and c is the light velocity. In practical conditions, harmonic modulation of the electron beam can be arranged by its preliminary bunching in the periodic waveguide or by using the laser emission.[20]

As is known,[8] the electromagnetic field of the beam (1) in the free space is H-polarized, and

$$H_z^0(x, y) = A \,\mathrm{sign}(y - h) e^{-q|y-h|} e^{i(k/\beta)x}, \tag{2}$$

where $q = k\gamma/\beta$, $\gamma = (1 - \beta^2)^{1/2}$, function $\mathrm{sign}(\cdot) = \pm 1$ is the sign of the expression in the brackets, time dependence is omitted, and $A > 0$ is a constant. This is a surface wave, which travels along the beam trajectory in the $+x$-direction and decays exponentially in the normal direction. It has a finite jump corresponding to the current at the beam trajectory. Note that the field (2) is an antisymmetric function of the coordinate y with respect to the beam trajectory that is a drastic difference from more conventional in optics plane-wave field, which is symmetric with respect to the propagation direction.

III. PROBLEM FORMULATION AND BASIC EQUATIONS

Consider a photonic molecule formed by two identical circular dielectric nanowires (#1 and #2) separated by distance L between their axes, with the same radius a and refractive index $\alpha = \sqrt{\varepsilon}$ (with ε being the relative dielectric permittivity). We assume that the electron beam (1) moves between the wires in parallel to the x axis at the distance h from it. Hence, the beam separation from the lower (upper) wire surface is $d = L/2 - a \pm h$. The Cartesian and the local and global polar coordinates are shown in Fig. 1.

The formulation of the 2D boundary-value problem for the unknown scattered field involves the Helmholtz equation off the wire contours of cross section, the penetrable-boundary conditions at these contours, the Sommerfeld radiation condition at infinity, and the local condition of the power finiteness. These conditions guarantee the solution uniqueness.

The above formulated PM configuration has been considered in a number of publications; however, to the best of our knowledge, it has not been studied with the electron-beam field (2) as a given excitation field. Here, the approximate numerical techniques like those referred in Ref. 25 and commercial finite-difference time-domain codes[26] are important for engineering applications, however, not enough accurate if studying the fundamental wave effects such as sharp resonances. Therefore, we follow the semianalytical technique first introduced by Twersky[27] and further improved in Refs. 3, 28, and 29. This technique exploits the circular shape of the boundaries

of wire cross sections and combines the expansion of the field function in the azimuth Fourier series (in the local polar coordinates of each wire) with the addition theorems for the Bessel functions. It enables one to reduce the scattering problem to the infinite-matrix equation for the expansion coefficients. The important correction, introduced in Refs. 3, 28, and 29, is the rescaling of that matrix equation to cast it to the Fredholm second-kind form. This correction guarantees the convergence of the numerical solution, in the mathematical sense.

Guided by these considerations, we expand the field in terms of the azimuth-coordinate Fourier series inside each wire

$$H^{\mathrm{int}(p)}(r,\varphi)=\sum_{m=-\infty}^{\infty} y_m^{(p)} J_m(k\alpha r_p)\exp(im\varphi_p),\quad r_p<a,\quad p=1,2. \tag{3}$$

In the presence of the twin scatterers, the total field in the external domain has the form of the sum

$$H^{ext}=H^0+H^{sc}, \tag{4}$$

$$H^{sc}(r,\varphi)=\sum_{p=1,2}\sum_{m=-\infty}^{+\infty} z_m^{(p)} H_m^{(1)}(kr_p)\exp(im\varphi_p),\quad r_p>a, \tag{5}$$

where $J_m(\cdot)$ and $H_m(\cdot)$ are the Bessel and Hankel first-kind functions, and (r_p,φ_p), $p=1,2$ are the local polar coordinates of the wires.

Expressions (3) and (5) satisfy the Helmholtz equation, the local power finiteness condition, and the radiation condition. To determine the unknown expansion coefficients, these expressions are substituted to the boundary conditions at the contours of the wires. Here, the addition theorems for the Bessel and Hankel functions are used as in Refs. 3 and 27–29. After the exclusion of the coefficients $y_n^{(p)}$, we obtain two coupled infinite-matrix equations for the remaining coefficients

$$z_m^{(1,2)}+\sum_{n=-\infty}^{+\infty} z_n^{(2,1)}(\pm i)^{n-m}V_m(P_m)^{-1}J_n(ka)H_{m-n}(kL) = -[f_m^{(1,2)}(ka)J'_m(k\alpha a)\alpha - J_m(k\alpha a)f'^{(1,2)}_m(ka)](P_m)^{-1}, \tag{6}$$

replace z_m^(1,2) with z~_m^(1,2) = z_m^(1,2)J_m(ka)

$$V_m=\alpha J_m(ka)J'_m(k\alpha a)-J'_m(ka)J_m(k\alpha a), \tag{7}$$

$$P_m=J_m(ka)[\alpha H_m(ka)J'_m(k\alpha a)-H'_m(ka)J_m(k\alpha a)], \tag{8}$$

$$f_m^{(1,2)}=\mp A\exp[-q(L/2\pm h)]i^m J_m(ka)(1\mp\gamma)^m\beta^{-m}, \tag{9}$$

where the superscript of the Hankel function is omitted and the prime means the differentiation in argument.

Inspection of (6) shows that the diagonal matrix elements of the first (second) block of (6) characterize the scattering by, respectively, the first (second) wire in the free space, and the off-diagonal elements characterize the optical interaction. Note that the off-diagonal elements are not zero and hence the interaction is always present and decays rather slowly, as $O[1/(kL)^{1/2}]$ if $kL\to\infty$.

The obtained set (6) is a Fredholm second-kind infinite-matrix equation (see Refs. 3, 28, and 29) due to the fact that $\sum_{m,n=-\infty}^{+\infty}|A_{mn}^{(1,2)}|^2<\infty$ and $\sum_{m=-\infty}^{+\infty}|B_m^{(1,2)}|^2<\infty$, where the matrix elements $A_{mn}^{(1,2)}$ and the right-hand part elements $B_m^{(1,2)}$ follow from (7) to (9). Then, the Fredholm theorems guarantee that its numerical solution (after truncation to finite order M) converges to the exact solution. To obtain 5 correct digits in the near field, one has to take $M\geq k\alpha a+5$ (and more if the airgap $L-2a$ gets much smaller than a).

IV. SCATTERING AND ABSORPTION CROSS SECTIONS

On using the large-argument asymptotic expressions for the Hankel functions, the scattered field in the far zone ($r\to\infty$) takes the form of a cylindrical wave, $H^{sc}(r,\varphi)=(2/i\pi kr)^{1/2}\Phi(\varphi)\exp(ikr)$, where the far-field angular scattering pattern depends on the coefficients $z_m^{(1,2)}$ as

$$\Phi(\varphi)=\Phi_1(\varphi)+\Phi_2(\varphi),\quad \Phi_{1,2}(\varphi)=\exp(\mp\tfrac{1}{2}ikL\sin\varphi)\sum_{m=-\infty}^{+\infty}(-i)^m J_m(ka)z_m^{(1,2)}\exp(im\varphi). \tag{10}$$

replace z_m^(1,2) with z~_m^(1,2)

Then, the total scattering cross section is found as

$$\sigma_{sc}=\frac{2}{\pi kA^2}\int_0^{2\pi}|\Phi(\varphi)|^2 d\varphi. \tag{11}$$

If the dielectric wires are lossy, then, besides the scattering, a part of the power of the incident field is absorbed in PM. This is characterized by the absorption cross section (ACS), which is found from the integration of the normal component of the time-averaged Poynting vector over the contours of the wires. This leads to the following equation:

$$\sigma_{abs}=\frac{2\pi a}{|\alpha|^2A^2}\sum_{m=-\infty}^{\infty}\left(|y_m^{(1)}|^2+|y_m^{(2)}|^2\right)\mathrm{Im}\left[\alpha J_m(k\alpha a)J'_m(k\alpha^* a)\right], \tag{12}$$

where

$$y_m^{(1,2)} J_n(k\alpha a) = z_m^{(1,2)} H_m(ka) + \sum_{n=-\infty}^{+\infty} (\mp i)^{(n-m)} z_n^{(2,1)} J_n(ka) H_{m-n}(kL) + f_m^{(1,2)}. \tag{13}$$

Thus, on solving the matrix equation (6) truncated to finite order M, one can calculate the scattering and absorption cross sections and the near- and far-field patterns. Note that the accuracy of the calculation of the near field and hence the ACS is the same as the accuracy of solving (6). However, the accuracy of calculation of the far-field angular pattern (10) and the TSCS (11) is approximately by an order of magnitude better because of the presence of the Bessel functions, which decay exponentially with n if $n > ka$.

Note that the sum of TSCS and ACS is called the extinction cross section.[30] Thanks to the Complex Poynting Theorem applied to the total field function and its complex conjugate, the extinction of the considered PM can be connected to the far-field values in certain complex directions. Here, it is necessary to introduce the complex-valued angles of incidence of the wave (2) in the upper and lower half-spaces, $\psi_{1,2}$, such that

$$\cos\ \psi_{1,2} = 1/\beta, \quad \sin\ \psi_{1,2} = \pm i\gamma/\beta. \tag{14}$$

Then, the real part of the expression, which follows from the Complex Poynting Theorem reduces to

$$\sigma_{sc} + \sigma_{abs} = -\frac{4}{kA^2} \mathrm{Re}[\Phi_1(\psi_1) + \Phi_2(\psi_2)] \tag{15}$$

or, with an account of (10),

$$\sigma_{sc} + \sigma_{abs} = -\frac{4}{kA^2} e^{-qL/2} \mathrm{Re} \sum_{m=-\infty}^{+\infty} (-i^m) J_n(ka) \left[z_n^{(1)} e^{-qh} \left(\frac{1-\gamma}{\beta} \right)^m + z_n^{(2)} e^{qh} \left(\frac{1+\gamma}{\beta} \right)^m \right]. \tag{16}$$

replace z_m^(1,2) with z~_m^(1,2)

The obtained expression plays the role of the optical theorem for the diffraction radiation excited by the electron beam (1) flowing between the wires of a twin-wire PM. If the TSCS value has been found, then the ACS value can be determined from (16) instead of (12). Comparison of two values of ACS, found from (12) and (16), can be viewed as a partial validation of the solution correctness. Still, their coincidence is only a necessary condition of correctness; however, it is not a sufficient one. The sufficient test is provided by the verification of the fulfillment of the boundary conditions.

In our work, the optical theorem has been satisfied at the level of machine precision and the boundary conditions have been satisfied with the same accuracy as the solution of the matrix equation (6), controlled by the truncation order M. Additional validation has been provided by the fact that if the relative dielectric permittivity of the wire #2 is set to be 1, then the computed TSCS and ACS are the same as for a single dielectric wire excited by the beam (1), where the full-wave analytical solution is available.[12]

V. NUMERICAL RESULTS

In computations, we are looking for the features of the DR associated with twin-cavity PM configuration that can be used for the detection of the shift of the beam trajectory from the central position between the dielectric wires. We are also interested in seeing the effect of the relative beam velocity, β, on the DR.

Here, we keep in mind that the modes of twin-wire PM (Fig. 1) are in fact "supermodes" built on the natural modes of each separate circular wire and optically coupled in four possible ways because of the two-fold symmetry. The reason of the splitting to quartets of supermodes is that the modes in a stand-alone circular cavity are double degenerate; however, this degeneracy is removed by bringing another circular cavity. Each supermode family has certain symmetry or antisymmetry of its field pattern with respect to each of the symmetry lines; therefore, they are classified usually as "x-even, y-even" (EE), "x-even, y-odd" (EO), "x-odd, y-even" (OE), and "x-odd, y-odd" (OO). If the electron beam flows along

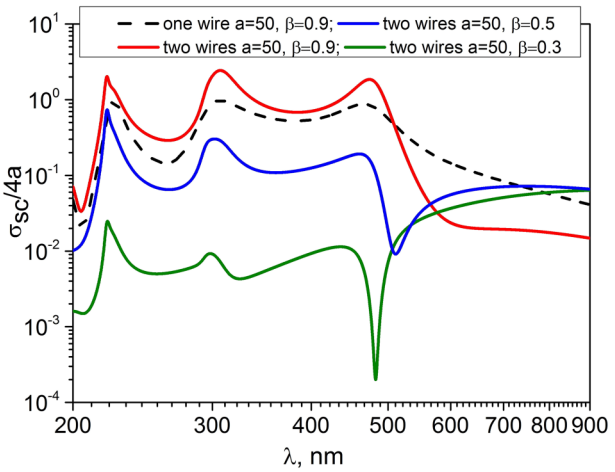

FIG. 2. Normalized TSCS of the 50-nm in radius one (dashed curve) and two silicon nanowires vs the wavelength in the visible range, for several values of the electron relative velocity β. The beam flows along the x axis ($h = 0$).

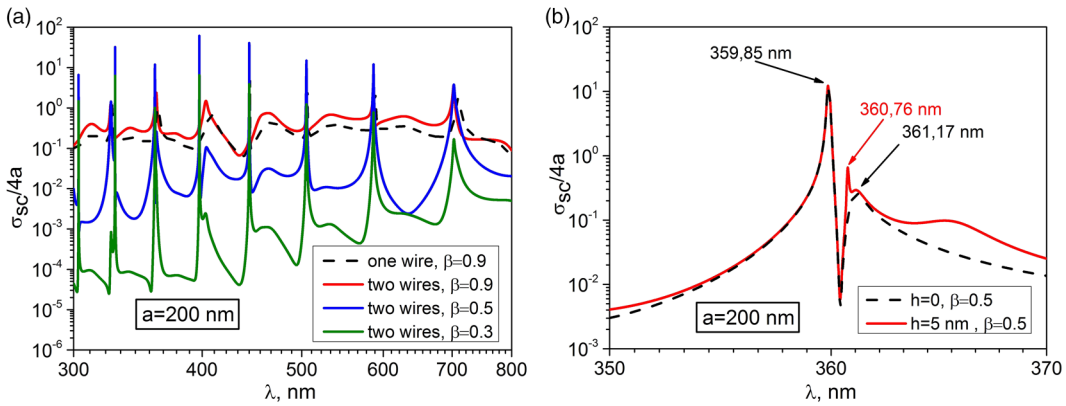

FIG. 3. The same as in Fig. 2, however, for one (dashed curves) and two (solid curves) silicon nanowires of the 200-nm radius (a) and a zoom of the TSCS spectra for in the wavelength range from 350 nm to 370 nm (b).

the x axis, i.e., exactly in the middle between the dielectric wires, then its field (2) is an antisymmetric function of y with respect to $y = 0$. Such incident field is able to induce only the resonances on the modes of the (EO) and (OO) families, the supermodes of the other two families, (EE) and (OE), remain "dark." The latter-mode resonances can be expected to start shining if the beam trajectory shifts from the central position, i.e., if $h \neq 0$. This effect can potentially serve as a marker for beam position monitoring.

We start our numerical experiments from the PM made of two subwavelength wires with $a = 50$ nm, and $\varepsilon = 12$ ($\alpha = 3.4641$). Such a material is similar to silicon or GaAs that have very small losses in the visible range, so that, at first, we neglect them. The airgap between wires is 20 nm. Figure 2 demonstrates the dependences of the normalized total scattering cross section (TSCS) on the beam modulation wavelength, for one and two thin subwavelength nanowires with the beam shift $h = 0$ nm and several values of the beam velocity β. As already mentioned, stand-alone circular dielectric nanowire is a convenient reference scatterer, for which the DR problem can be solved analytically similar to the plane-wave scattering—see Ref. 12 for details.

For all β, the plots of TSCS show three distinctive peaks at $\lambda = 225$ nm, 306 nm, and 464 nm with smooth shapes. The intensity of DR decays if β gets smaller, i.e., for a nonrelativistic beam, because its field (2) becomes compressed to the beam trajectory. The resonance peaks are broad that tells that the corresponding natural modes have small Q-factors. This is apparently the reason that no splitting into doublets of the (EO) and (OO) supermodes is visible so that each peak is a collective resonance on both of them.

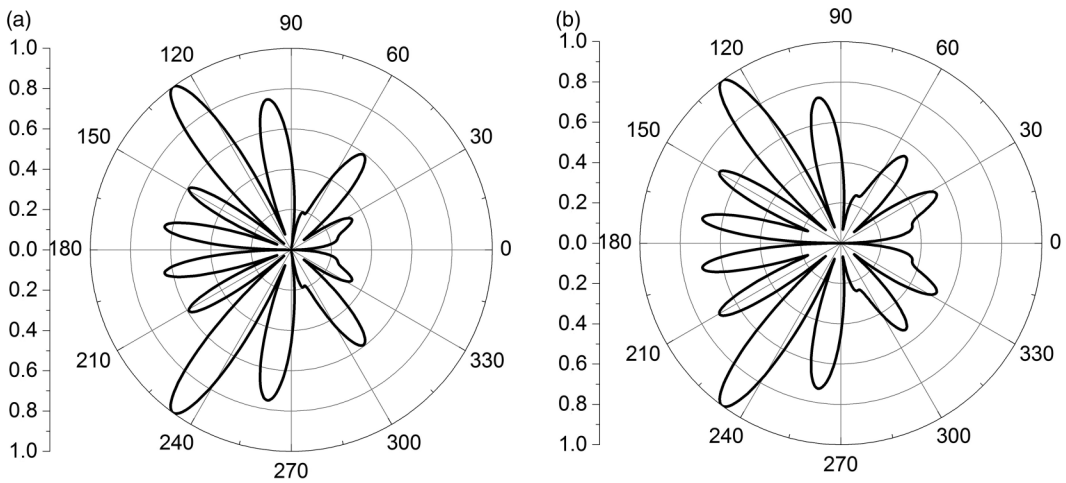

FIG. 4. Symmetric beam excitation. In-resonances normalized far-field scattering patterns of twin silicon nanowires of the radius $a = 200$ nm, $L = 120$ nm, $h = 0$, and $\beta = 0.5$ at $\lambda = 359.85$ nm (a) and 361.17 nm (b).

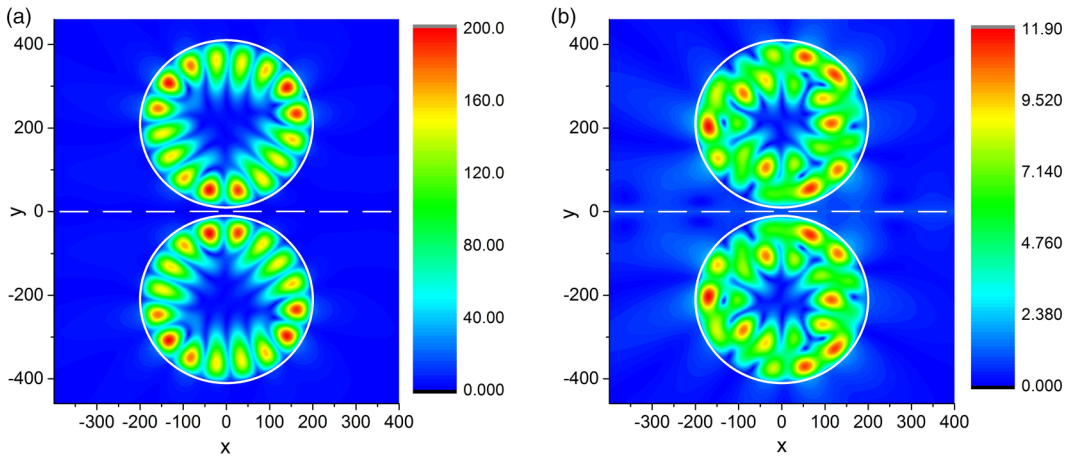

FIG. 5. Symmetric beam excitation. In-resonances near-field patterns of twin silicon nanowires of the radius $a = 200$ nm, $L = 120$ nm, $h = 0$, and $\beta = 0.5$ at $\lambda = 359.85$ nm (a) and 361.17 nm (b).

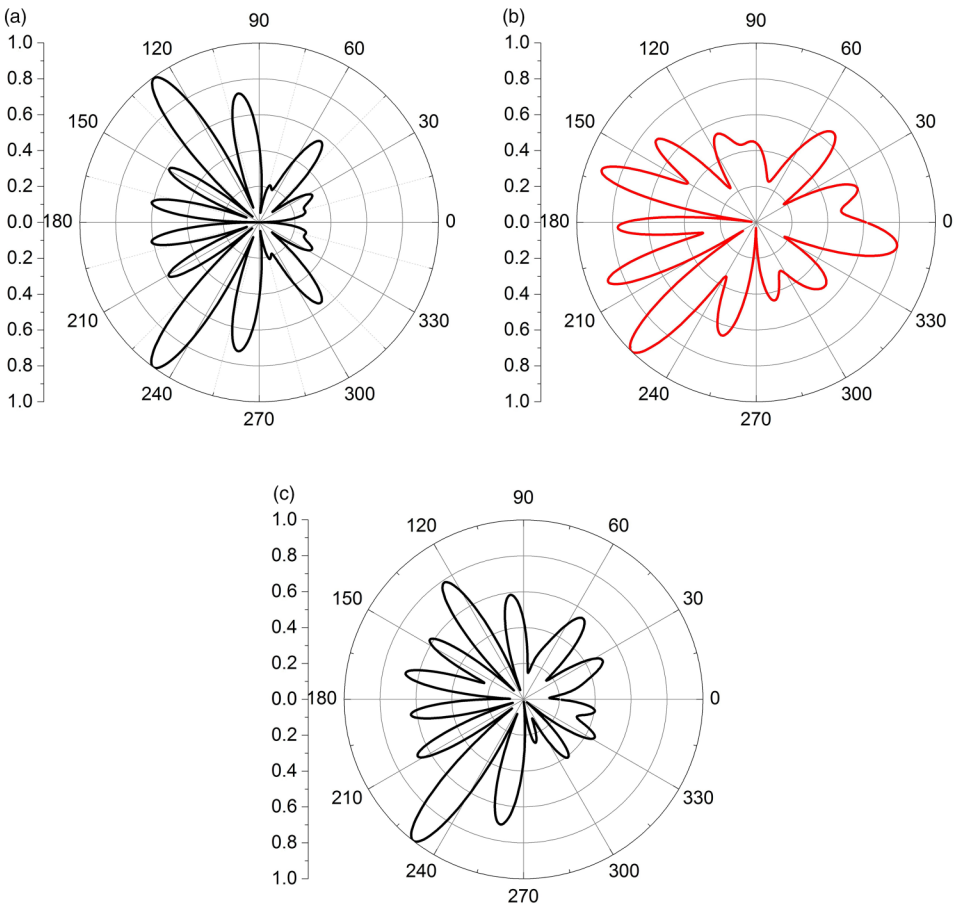

FIG. 6. Nonsymmetric beam excitation. The same as in Fig. 4 for $a = 200$ nm, $L = 420$ nm, $h = 5$ nm, and $\beta = 0.5$ at $\lambda = 359.85$ nm (a), 360.76 nm (b), and 361.17 nm (c).

Moreover, if the beam trajectory is shifted from the x axis, these peaks do not split further, again because of the low Q-factors of the (EE) and (OE) supermodes, which are "dark" if $h = 0$ but became "bright" if $h \neq 0$. They give an idea that too thin dielectric wires, even if made from high refractive index material, are not a promising configuration for the beam-diagnostics applications.

Therefore, the plots in Fig. 3(a) demonstrate the wavelength scans of TSCS for much thicker silicon nanowire PM with $a = 200$ nm and the same airgap of 20 nm. As one can see, in this case, there are multiple resonances within the visible range (i.e., for λ from 300 nm to 800 nm). A zoom of the part of the spectrum near to 360 nm is shown in Fig. 3(b) for the beam velocity $\beta = 0.5$ and two beam shifts, $h = 0$ and $h = 5$ nm.

According to Ref. 3, the quartets of supermodes actually form two tight doublets: one of the (OO) and (EO) families modes and another of the (EO) and (EE) families. Close inspection shows that the complex poles underlying the higher-Q peak of TSCS for $h = 0$ at the wavelengths of 359.85 nm in Fig. 3(b), correspond to the supermode $H_{8,1}^{OO}$ and apparently not resolved sister-mode $H_{8,1}^{EO}$. Similar to that, a broader peak at 361.17 nm corresponds to the lower-Q supermode $H_{7,2}^{OO}$ and its not resolved sister-mode $H_{7,2}^{EO}$. This interpretation is fully supported by the in-resonance normalized far-field angular patterns and the near-field patterns shown in Figs. 4 and 5, respectively, for the symmetric excitation of twin-wire PM ($h = 0$). The beam trajectory is indicated by the dashed line. In each peak, the supermodes of the (OO) family dominate in the total field.

What is most important from the viewpoint of applications in BPM design, if the beam trajectory is shifted from the x axis, then new additional peaks of TSCS appear. This is visible on the zoomed spectrum shown in Fig. 3(b) for $h = 5$ nm: an additional sharper peak starts shining at 360.76 nm and a broad peak appears at 365.5 nm. The corresponding in-resonance far-field angular patterns and the total near-field patterns are depicted in Figs. 6 and 7, respectively.

Note that the pattern in Fig. 6(a) is very close to the pattern in Fig. 4(a) and that in Fig. 7(a)—to the one in Fig. 5(a). The same is

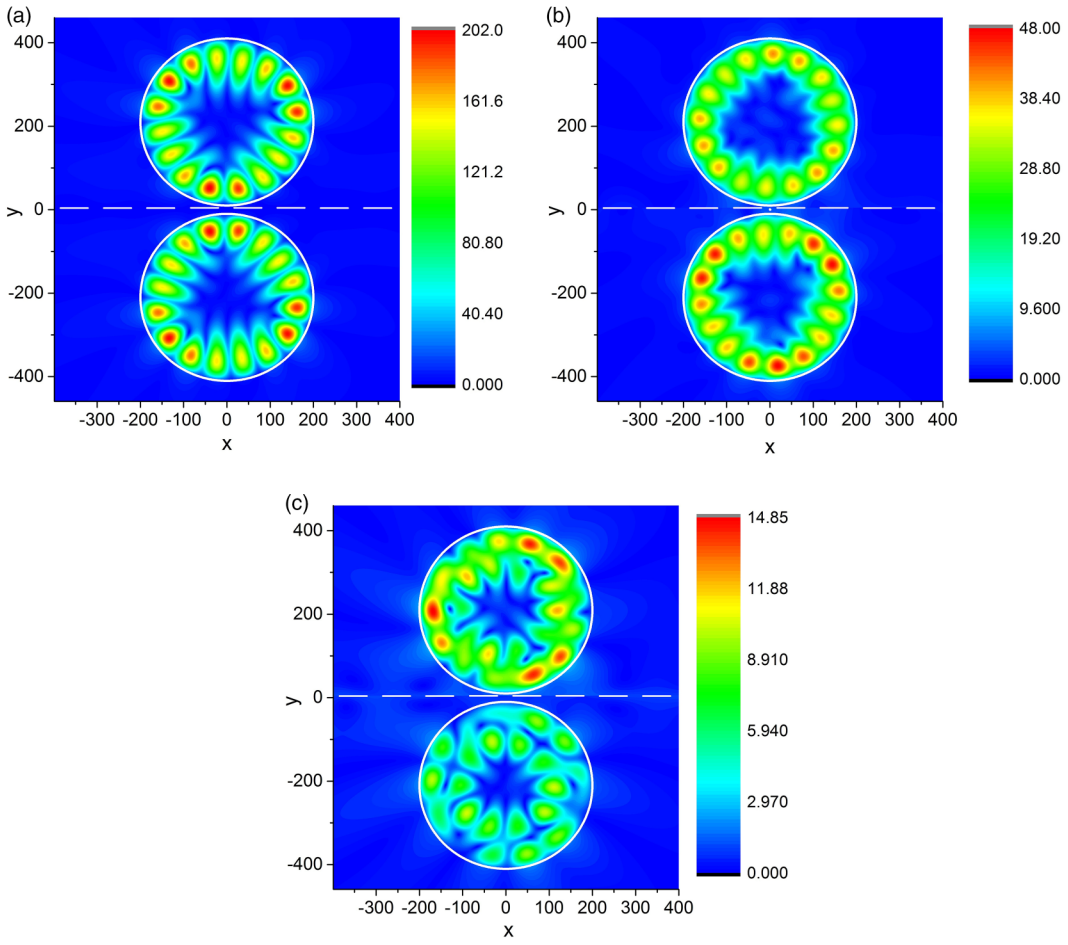

FIG. 7. Nonsymmetric beam excitation. The same as in Fig. 5 for $a = 200$ nm, $L = 420$ nm, $h = 5$ nm, and $\beta = 0.5$ at $\lambda = 359.85$ nm (a), 360.76 nm (b), and 361.17 nm (c).

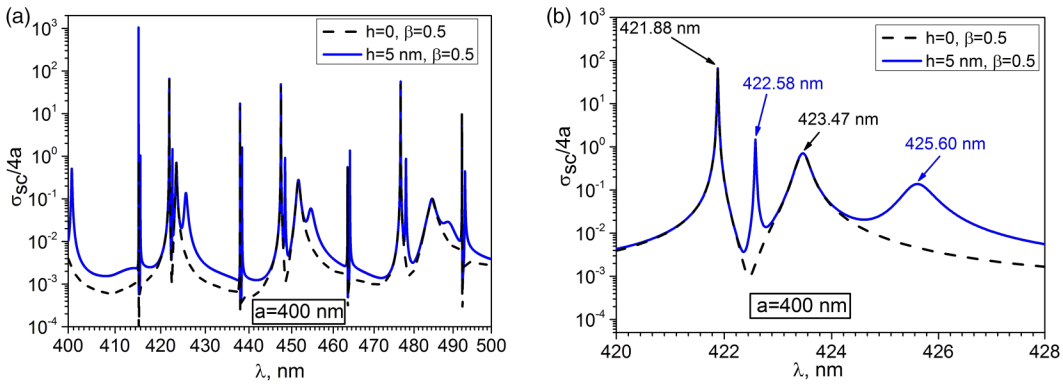

FIG. 8. Normalized TSCS of PM on twin silicon nanowires of 400-nm radius with 20-nm airgap vs the wavelength, for the electron relative velocity $\beta = 0.5$ and two values of the shift distance h.

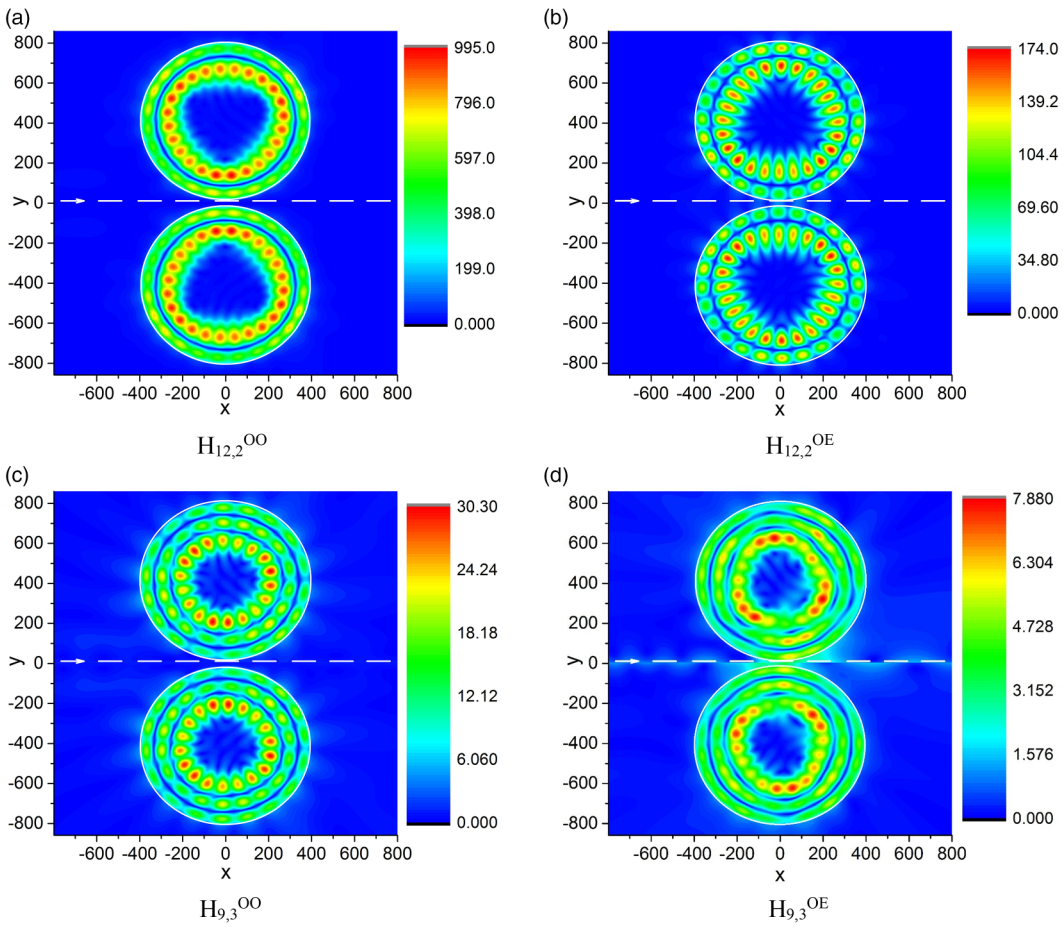

FIG. 9. Nonsymmetric excitation. In-resonances near-field patterns of twin silicon nanowires of the radius $a = 400$ nm, $L = 820$ nm, $h = 5$ nm, and $\beta = 0.5$ at $\lambda = 421.88$ (a), 422.58 (b), 423.47 (c), and 425.60 nm (d).

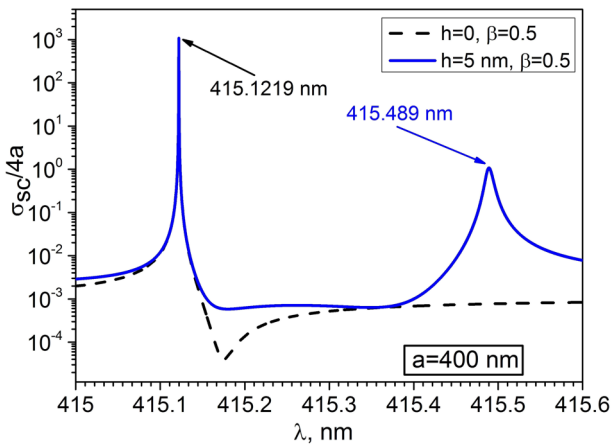

FIG. 10. Zoom of TSCS curves from Fig. 8(a) between $\lambda = 415$ nm and 415.6 nm.

visible for the patterns shown on panels (c) of Figs. 6 and 7 and panels (b) of Figs. 4 and 5, respectively. This leads to the conclusion that the supermodes with the fields, antisymmetric with respect to y, are weakly sensitive to the shift h of the beam trajectory. The explanation of this property can be seen in the fact that these modes have zero values of their H-fields on the x axis and hence it is much better compatible with the incident field (2) than of the y-even mode families.

In contrast, the patterns shown in Figs. 6(b) and 7(b) correspond to the new resonance at 360.76 nm, which is absent if $h = 0$. They demonstrate that this is the resonance on the supermode $H_{8,1}^{EO}$, with some admixture of its not resolved sister-mode $H_{8,1}^{EE}$, which has smaller contribution. Similar conclusions can be reached for the broad peak at 365.5 nm, not existent at $h = 0$.

To further support these conclusions, we have computed the TSCS spectra for the symmetric and shifted beam excitation of the twin-wire PM with even larger (but still nanoscale) silicon resonators of 400-nm radius. The corresponding plots are presented in Fig. 8(a) for $\beta = 0.5$ and the shift values $h = 0$ and $h = 5$ nm in the range of wavelengths between 400 nm and 500 nm, and a zoom around 423 nm is shown in Fig. 8(b). Like in the previous example, the TSCS of the PM excited by symmetrically flowing beam demonstrates two resonance peaks, while the non-symmetrically excited PM—four resonance peaks.

As we could already see, the interpretation of the resonances is best achieved via visualizing the near-field patterns. The four in-resonance field patterns corresponding to the four peaks of TSCS in Fig. 8(b) for the beam shifted by $h = 5$ nm are presented in Fig. 9.

They demonstrate convincingly the fields dominated by the higher-Q supermodes $H_{12,2}^{OO}$ at 421.9 nm and $H_{12,2}^{OE}$ at 422.6 nm in the sharp peaks of TSCS, and the lower-Q supermodes $H_{9,3}^{OO}$ at 423.5 nm and $H_{9,3}^{OE}$ at 425.6 nm—in the broader peaks of TSCS. In each case, the pattern is slightly distorted by the presence of not fully resolved sister-supermode of the x-even family. Here, similarly to the previous example with 200-nm in radius twin-wire PM, the appearance of the peaks on the y-even modes $H_{12,2}^{OE}$ and $H_{9,3}^{OE}$ can serve as a marker of the beam deviation from the center of the 20-nm airgap.

Finally, we have analyzed in detail the sharper peaks of TSCS in Fig. 8(a) near to the wavelength of 415 nm. The zoomed area around this wavelength is shown in Fig. 10 for the shifted by 5 nm and not shifted trajectories of the electron beam with $\beta = 0.5$. Similar to the previous analysis, the sharper peak on the $H_{16,1}^{OO}$ supermode at $\lambda = 415.1219$ nm is present in both cases and keeps the same shape, and the other peak on the $H_{16,1}^{OE}$ supermode at 415.489 nm appears only if the beam trajectory is shifted. The supermode type identification is based on the visualization of the near-field patterns in these two resonances, presented in Fig. 11.

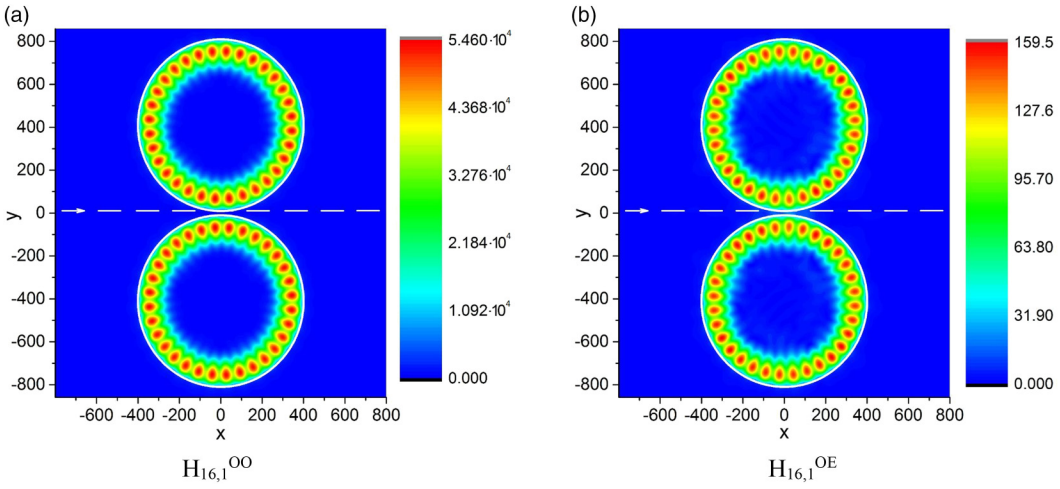

FIG. 11. Nonsymmetric excitation. In-resonances near-field patterns of twin silicon nanowires of the radius $a = 400$ nm, $L = 820$ nm, $h = 5$ nm, and $\beta = 0.5$ at $\lambda = 415.1219$ nm (a) and 415.489 nm (b).

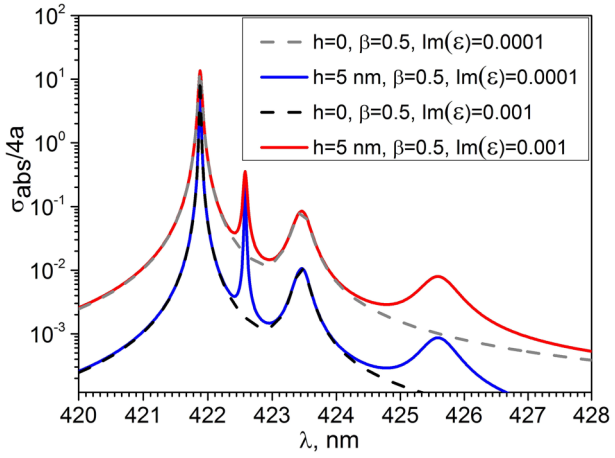

FIG. 12. Normalized ACS of PM on twin silicon nanowires of 400-nm radius with 20-nm airgap vs the wavelength, for the electron relative velocity $\beta = 0.5$ and two values of the shift distance h.

Thus, such an effect is also a marker of the beam trajectory deviation from the central (symmetrical) position.

So far we have been discussing the numerical results computed with the lossless dielectric cavities. In order to obtain a vision of the role played by the losses, now we introduce small bulk material losses, Im ε, in the 400-nm in radius wires and compute the ACS as a function of the wavelength—see Fig. 12. The PM and the electron-beam parameters are taken the same as in Fig. 8(b).

As one can see, the ACS spectra show the resonance peaks at the same wavelengths as on the plots of TSCS, which are not shown here because for so small bulk losses they overlap with the curves in Fig. 8(b). The maximum value of the absorption is achieved in the resonance on the most high-Q mode, $H^{OO}_{12,2}$; however, it is still by the order of magnitude lower than the resonance scattering [compared with Fig. 8(b)]. Similar to the scattering cross-section, two additional peaks of the absorption appear if the beam trajectory deviates from the airgap center, due to now "bright" y-even modes $H^{OE}_{12,2}$ and $H^{OE}_{9,3}$. If the bulk losses in the dielectric material are taken 10 times greater, 10^{-3} instead of 10^{-4}, then the ACS curves also rise by approximately an order, except the high-Q resonances where this rise is canceled by the Q-factor, which in this case is inverse proportional to the bulk losses.

VI. CONCLUSIONS

The field of the periodically modulated, in density, electron beam can be viewed as a surface wave propagating along the beam trajectory. This wave field has unusual optical properties: it is antisymmetric with respect to the beam trajectory. It induces the secondary currents on the local obstacles that radiate in the background medium even if the beam does not touch them. In fact, a nearby scatterer plays the role of an optical nanoantenna, which makes the beam of charged particles visible. We have studied, using an accurate and mathematically grounded in-house code, the beam excitation of a photonic molecule formed by a pair of identical nanowires made of high refractive index dielectric material, with a beam flowing between the wires. Such a PM behaves as a composite optical open resonator, which supports supermodes built on the natural modes of each cavity combined together according to the two-fold symmetry of this configuration. The emerging diffraction radiation is resonantly enhanced near each natural supermode wavelength. As we have found, if the beam trajectory shifts away from the central (i.e., symmetrical) position, then new peaks in the spectra of the scattering become visible. They are due to the resonances on the formerly "dark" supermodes, which are absent in the symmetric beam excitation. This effect can be important for applications related to the design of novel optical-range beam position monitors. Here, a question of the feasibility arises. In fact, today, the size of controllably manufactured subwavelength dielectric microcavities is measured in hundreds and dozens of nanometers. So, in principle, this is realistic. Besides, the scattering by a dielectric resonator with a fixed relative permittivity can be scaled up to larger sizes and wavelengths. For example, the curves presented in Figs. 8–11 for the wire radius 400 nm and the wavelengths of 400 nm to 500 nm are equally valid for the wire radius 4 mm and the wavelengths of 4 mm to 5 mm.

ACKNOWLEDGMENTS

D.O.Y. was supported by the IEEE Microwave Theory and Techniques Society via Pre-Graduate Scholarship and by the IEEE Antennas and Propagation Society via Pre-Doctoral Research Award that are acknowledged with gratitude.

REFERENCES

[1]M. Bayer, T. Gutbrod, J. P. Reithmaier, A. Forchel, T. L. Reinecke, P. A. Knipp, A. A. Dremin, and V. D. Kulakovskii, Phys. Rev. Lett. **81**, 2582 (1998).
[2]Y. Kara, T. Mukayama, K. Takeda, and M. Kuwata-Gonokami, "Photonic molecule lasing," Opt. Lett. **28**, 2437 (2003).
[3]E. I. Smotrova, A. I. Nosich, T. M. Benson, and P. Sewell, IEEE J. Sel. Top. Quant. Electron. **12**, 78 (2006).
[4]E. I. Smotrova, A. I. Nosich, T. M. Benson, and P. Sewell, Opt. Lett. **31**, 921 (2006).
[5]Y. Li, F. Abolmaali, K. W. Allen, N. I. Limberopoulos, A. Urbas, Y. Rakovich, A. V. Maslov, and V. N. Astratov, Laser Photon. Rev. **11**(2), 1600278 (2017).
[6]H.-J. Chen, J. Appl. Phys. **124**, 153102 (2018).
[7]S. J. Smith and E. M. Purcell, Phys. Rev. **92**, 1069 (1953).
[8]P. M. van den Berg, J. Opt. Soc. Am. **63**, 689 (1973).
[9]A. P. Potylitsyn, Phys. Lett. A **238**, 112 (1998).
[10]A. I. Nosich, Radiophys. Quant. Electron. **24**, 696 (1981).
[11]A. I. Boltonosov and V. G. Sologub, Sov. J. Commun. Technol. Electron. **33**, 133 (1988).
[12]D. O. Yevtushenko, S. V. Dukhopelnikov, and A. I. Nosich, Opt. Quant. Electron. **51**, 29 (2019).
[13]M. Castellano, Nucl. Instrum. Methods Phys. Res. **394**, 275 (1997).
[14]M. Castellano, V. A. Verzilov, L. Catani, A. Cianchi, G. Orlandi, and M. Geitz, Phys. Rev. E **63**, 056501 (2001).
[15]P. Karataev, S. Araki, R. Hamatsu, H. Hayano, T. Muto, G. Naumenko, A. Potylitsyn, N. Terunuma, and J. Urakawa, Phys. Rev. Lett. **93**, 244802 (2004).
[16]Y. A. Goponov, R. A. Shatokhin, and K. Sumitani, Nucl. Instrum. Methods A **885**, 134 (2018).
[17]L. Bobb, R. Kieffer, T. Lefevre, S. Mazzoni, T. Aumeyr, P. Karataev, M. Billing, J. Conway, and J. Shanks, Phys. Rev. Accel. Beams **21**, 03801 (2018).
[18]T. Muto, S. Araki, R. Hamatsu, H. Hayano, T. Hirose, P. Karataev, G. Naumenko, A. Potylitsyn, and J. Urakawa, Phys. Rev. Lett. **90**, 104801 (2003).
[19]N. Talebi, J. Opt. **19**, 103001 (2017).

[20]K. J. Leedle, A. Ceballos, H. Deng, O. Solgaard, R. F. Pease, R. L. Byer, and J. S. Harris, Opt. Lett. **40**, 4344 (2015).
[21]M. Riso, M. Cuevas, and R. A. Depine, J. Opt. **17**, 075001 (2015).
[22]E. A. Velichko, J. Opt. **18**, 035008 (2016).
[23]M. Cuevas, M. A. Riso, and R. A. Depine, J. Quant. Spect. Radiat. Transf. **173**, 26 (2016).
[24]S. V. Dukhopelnikov, R. Sauleau, and A. I. Nosich, "Integral equation analysis of terahertz RCS of circular dielectric rod with partial graphene cover", IEEE Trans. Antennas Propagat. (unpublished).
[25]S. Deng and W. Cai, J. Opt. Soc. Am. A **22**, 952 (2005).
[26]S. Arslanagic and O. Breinbjerg, Materials **4**, 117 (2011).
[27]V. Twersky, J. Appl. Phys. **23**, 1099 (1952).
[28]D. M. Natarov, V. O. Byelobrov, R. Sauleau, T. M. Benson, and A. I. Nosich, Opt. Express **19**, 22176 (2011).
[29]D. M. Natarov, R. Sauleau, M. Marciniak, and A. I. Nosich, Plasmonics **9**, 389 (2014).
[30]C. F. Bohren and D. R. Huffman, *Absorption and Scattering of Light by Small Particles* (Wiley-VCN Publications, 2004).